5.1 INTRODUCTION

Lead [Pb(II) ion] considered as one of the most toxic metal which is found ubiquitously in water, air, and soil [Zheng *et al*. (2013)]. Lead show non-biodegradable nature and have ability to mimic the other biologically important metal ions such as calcium, iron, and zinc. Thus, the lead may interfere in various essential functions of the living organism leads to malfunctioning and induce lethal effects. Because of these qualities lead caused malfunctioning of different organs and can produce neurological, reproductive, and genotoxic disorders as well as can induce carcinogenicity in the human body [Kumar *et al.* (2014)]. In potable water, the lead concentration should be less than 0.01 mg/L [Ahmaruzzaman and Gupta (2011)]. Due to these toxic effects it is needed to be removed from the water. Thus, this chapter concerns with the adsorptive remediation of lead by GO/MgO nanocomposite from the water. The Magnesium oxide (MgO) nanoparticles are widely used as adsorbent due to its environmental benign nature, easy and cheap synthesis procedure [Yu *et al.* (2011)]. Literature showed many reports on the application of MgO as adsorbent as it shows high uptake capacity, non-toxicity and environmental friendly nature [Mahmoud *et al.* (2016), Hu *et al*. (2010) Dargahi *et al*. (2016), Yu *et al*. (2011)]. Carbon nanomaterials have been used as an excellent adsorbent for various types of pollutant which includes organic pollutants and heavy metals. They showed high adsorption performance due to their high reactivity, superior specific surface area, abundant active binding sites, and selectivity in aqueous solutions [Ruparelia *et al.* (2008), Rao *et al.* (2007), Stafiej & Pyrzynska (2007), Tawabini *et al.* (2010), Pyrzyńska & Bystrzejewski (2010), Kadirvelu *et al.* (2000), Goel *et al*. (2005)]. Among them, the Graphene oxide (GO) showed potential adsorption capacity for the variety of pollutants [Dervin *et al.* (2016), Wang *et al*. (2013)]. The GO find application in many biological and environmental

fields due to its exceptionally large surface area and the occurrence of plenty of oxygen functional groups on its surface [Yu *et al.* (2015)]. The functional group behaves as the binding sites for the pollutant ions, and the ions may interact via covalent bonding or by electrostatic interaction. In general graphene layers are prone to aggregate because of strong van der Waal interaction amongst the layers which leads to the reduction of surface area [Yang *et al.* 2012]. Thus, to inhibit the restacking of the GO layers, surface may be modified with metal oxide nanoparticles which prevent the aggregation of GO layers [Hao *et al.* (2012). However, the in-situ growth of metal oxide nanoparticles on the GO surface resisted its agglomeration and kept them in dispersed form. Therefore, the prepared nanocomposite of GO with metal oxide provides the robustness to the resultant nanocomposite. Thus, by preparing the nanocomposite of GO and MgO, we can utilize both the properties i.e. high surface area and adsorption properties of GO as well as MgO nanoparticles [Wang *et al*. (2012)]. In the current section of the thesis, simple precipitation method is being used to prepare the nanocomposite of GO and MgO (GO/MgO) which is expected to show high adsorption capacity for the lead. The influence of various parameters i.e. pH, temperature, initial lead concentration, adsorption time, and the adsorbent dose on the uptake capacity of the GO/MgO were also investigated. Moreover, detailed isotherm, thermodynamic and kinetic studies were also conducted.

5.2 MATERIAL AND METHOD

5.2.1 Synthesis of GO/MgO Nanocomposite

The detail procedure of synthesis of starting material GO is given in the chapter 2.For the preparation of GO/MgO nanocomposite, 50 mg GO was suspended into the 100 mL DW by ultrasonication for two h to produce GO dispersion. Further, 20 mL

aqueous solution of $Mg(NO_3)_2.6H_2O$ (0.04 M) was added to the above GO suspension and stirred at room temperature for 10 min. After that, 10 mL aqueous solution of NaOH (0.5M) was poured into the resulting reaction mixture in a drop-wise manner with stirring. Ultimately, the obtained solid product was washed with methanol and then by DW. The washed product was calcined at 250°C for four h. The pictorial representation of the synthesis of GO/MgO nanohybrid is shown in Figure.5.1

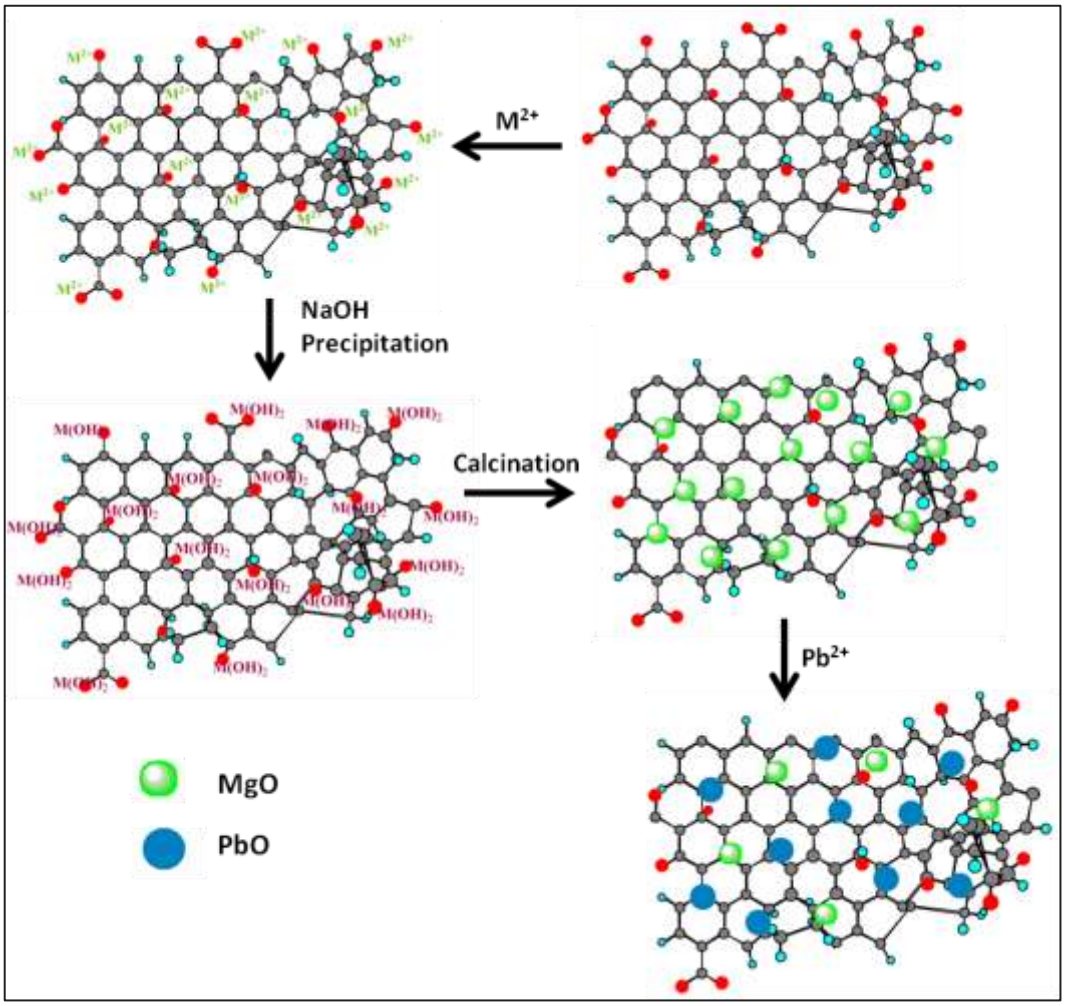

Figure 5.1 Schematic representation of synthesis of Graphene oxide magnesium oxide

5.2.2 Experimental methodology

The synthesis of GO/MgO nanocomposite and its physical as well as chemical properties were characterized with different characterization tools such as FT-IR, XPS, SEM, EDX, Raman spectroscopy, XRD, BET and pHzpc measurement. The prepared nanocomposite was utilized for lead removal by batch experimentation. The effect of different process parameters were studied by altering the solution pH (2-11), contact time (0-50 min), rGO/ZrO_2 dose (0.3-0.5 g/L), initial lead concentration (0-160 mg/L) and temperature (20-40°C). The detailed kinetic, isotherm and thermodynamic studies were also conducted.

5.3 CHEACHTERIZATION OF GO/MgO NANOCOMPOSITE

5.3.1 FTIR ANALYSIS

Figure 5.2 represent the FTIR spectrum of GO, MgO, and GO/MgO. The GO displayed its characteristic peaks corresponding to different functional groups of GO at 1080 cm^{-1} (alkoxy -C-O), 1285 cm^{-1} (epoxy -C-O), 1395 cm^{-1} (OH bending vibrations), 1640 cm^{-1} (aromatic C=C), 1724 and 1390 cm^{-1} (carboxyl –C=O and –C–O respectively). These peaks confirmed the presence of the various functional groups on the GO surface. The spectrum of MgO showed the peaks in the region of 400-850 cm^{-1} which are ascribed to the M-O and M-OH bending vibration of the metal oxide [Ai *et al.* (2012)] while, the peak at 1627 cm^{-1} was appeared due to the bending vibration of the physically adsorbed water [Wu *et al.* (2016)]. The FTIR spectrum of GO/MgO contains the peaks corresponding to both GO and MgO which confirmed the formation of GO/MgO nanohybrid.

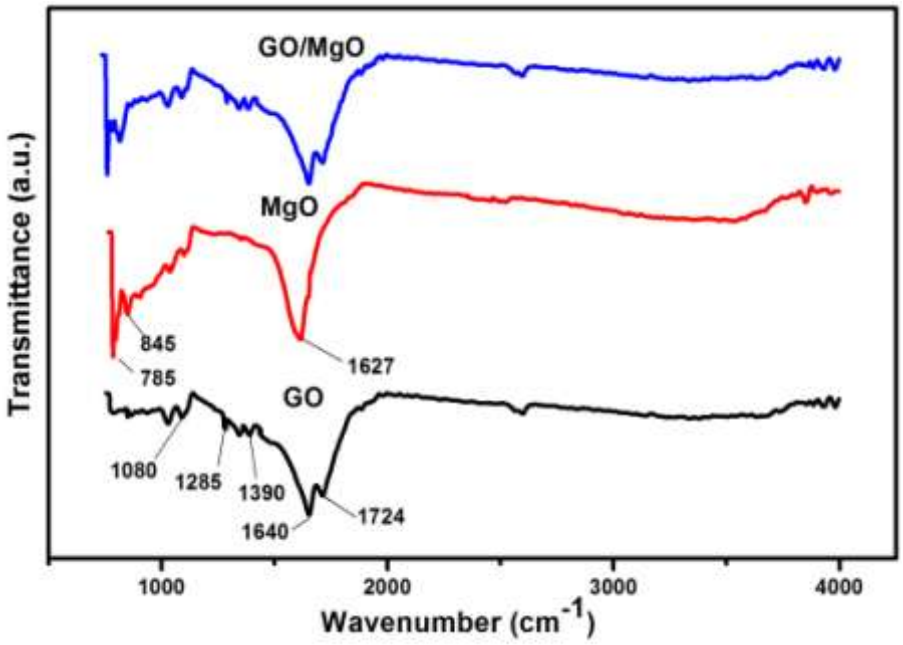

Figure 5.2 FT-IR spectra of GO, MgO and GO/MgO

5.3.2 XRD Analysis

The XRD pattern of the GO, MgO, and GO/MgO is shown in Figure 5.3. The peak at 2θ = 11.2° in the XRD pattern of the GO appeared due to the diffraction from 002 plane which is the characteristic pattern of the GO [Lee *et al.* (2011)]. The XRD pattern of the MgO nanocubes showed the feature peak corresponding to the cubic phase of MgO at 2θ = 36.78°, 42.84°, 62.12°, 74.53°, and 78.46°. These peaks were well matched with the JCPDS file no. 89-7746. After the formation of GO/MgO nanocomposite, the peak assigned for GO was shifted from 2θ = 11.2° to 2θ = 12.1 which may be occurred due to the interaction of Mg^{2+} ions with GO. Figure 5.3 also showed the XRD spectrum of the GO/MgO, in which the characteristic peaks of GO along with MgO both are present which confirm the successful formation of the desired nanocomposite.

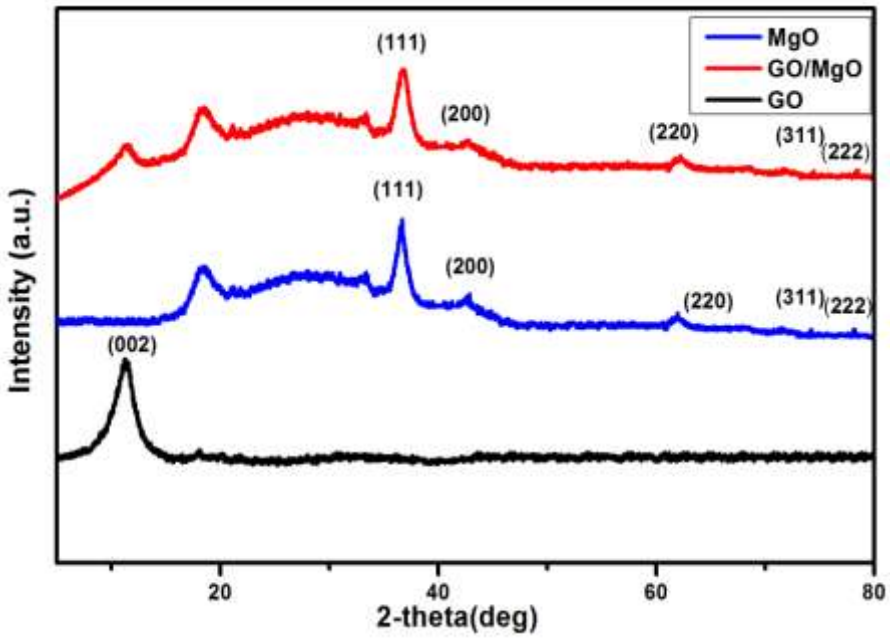

Figure 5.3 XRD pattern of GO, MgO, and GO/MgO

5.3.3 XPS Analysis

The XPS analysis is the most important and sensitive tool to investigate the oxidation state and composition of the material. The wide scan spectra of GO/MgO nanocomposite shown in Figure 5.4a which contain the characteristic peaks corresponding to the C1s, O1s, and Mg2p. Therefore, the presence of carbon, oxygen and magnesium in the nanocomposite was confirmed. The wide scan spectra of the adsorbent after the lead adsorption was also recorded and is given in Figure 5.4a which indicate the presence of lead on the surface of GO/MgO nanocomposite. Figure 5.4b represents the core level spectra of C1s which contained the featured gaussian peaks associated with the various functional groups of the GO. The peaks found at 285.20, 287.16 and 288.81 eV attributed to the C-C/C=C, C-OH, and COOH groups of GO [Singh *et al.* (2016)]. Furthermore, the high-resolution XPS spectrum of Mg2p is

shown in Figure 5.4c which showed two distinct peak corresponding to the Mg^{2+}(MgO) and Mg^{0} at 51.3 and 49.9 eV [Huang *et al*. (2010)].

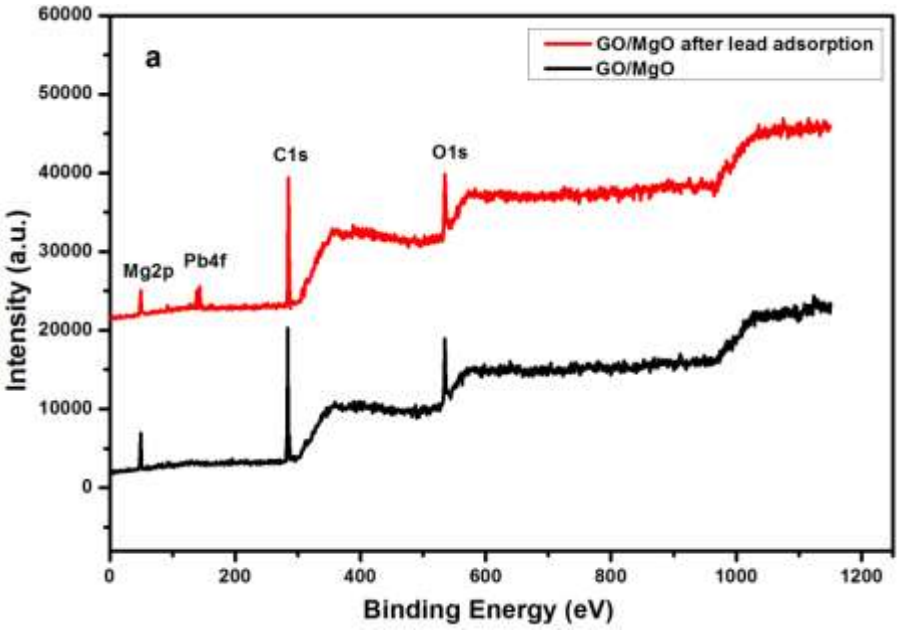

Figure 5.4a Wide scan XPS spectra of GO/MgO before and after adsorption

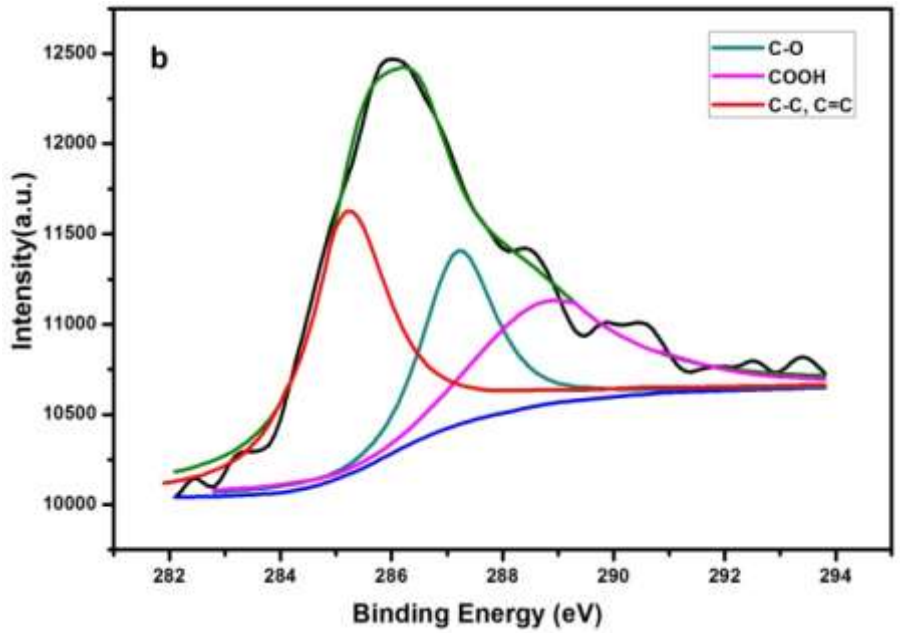

Figure 5.4b Core level C1s spectrum of GO

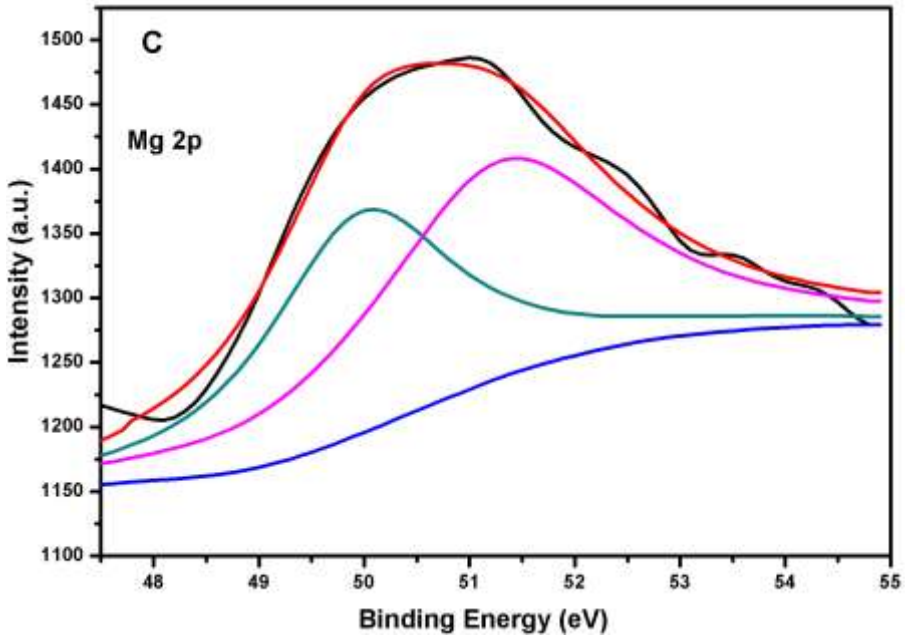

Figure 5.4c core level Mg 2p spectrum of Mg

5.3.4 SEM and EDX analysis

The typical morphology of GO is shown in Figure 5.5a in which wrinkled morphology of dense stacked GO layers is clearly seen [Yang *et al.* (2009)]. Whereas, Figure 5.5 b displayed the SEM image of the prepared GO/MgO nanocomposite in which the MgO nanoparticles are uniformly dispersed in the GO surface. Figure 5.5c, 5.5d is the high resolution SEM micrograph of the GO/MgO which revealed the presence of cubic shaped MgO nanoparticles with average size ~50 nm. Moreover, the EDX analysis was also performed to confirm the elemental composition of the as-prepared adsorbent before and after the lead adsorption.

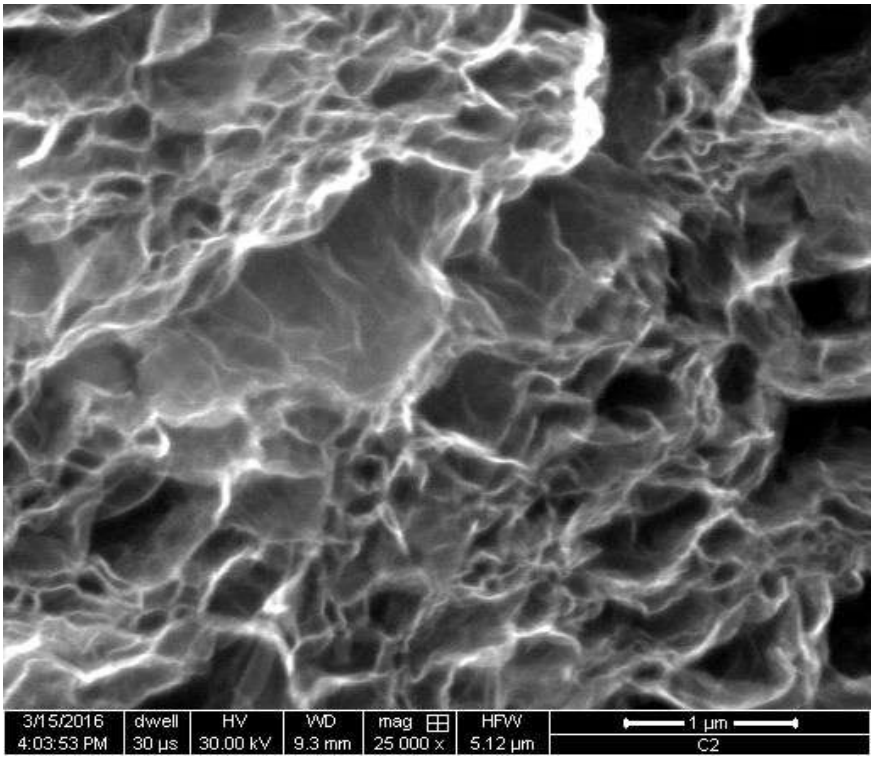

Figure 5.5a SEM image GO

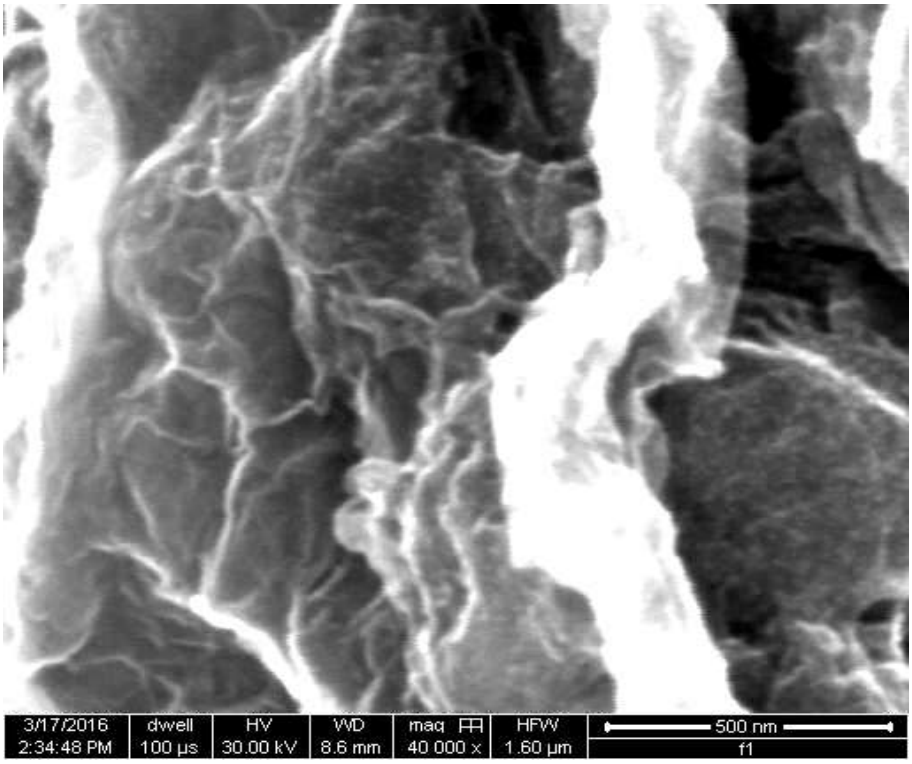

Figure 5.5b SEM image GO/MgO

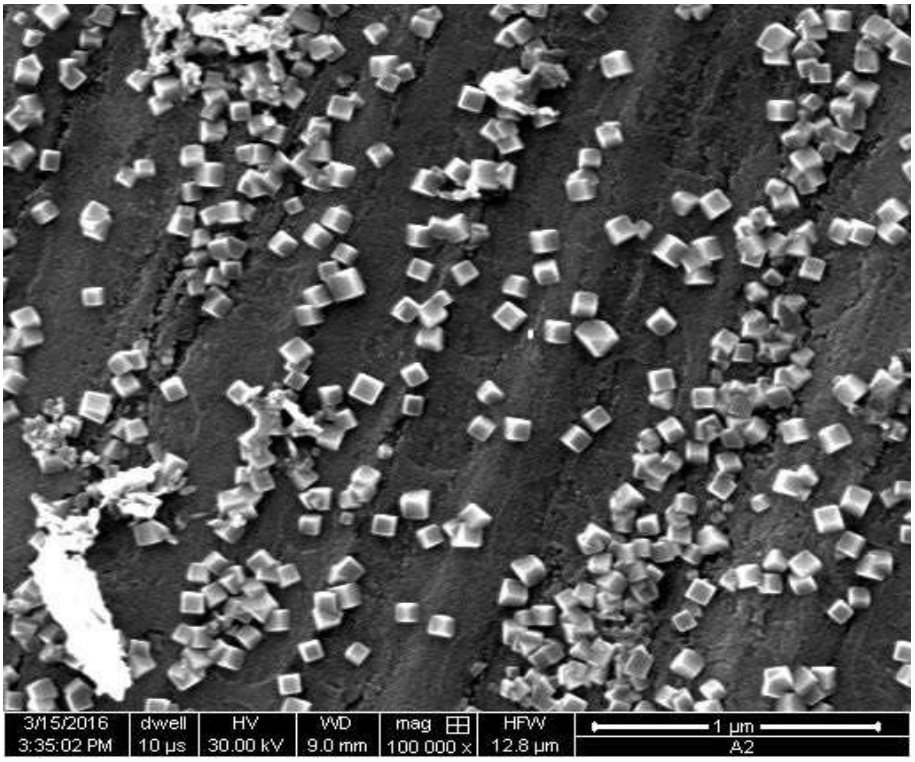

Figure 5.5c High resolution SEM image GO/MgO

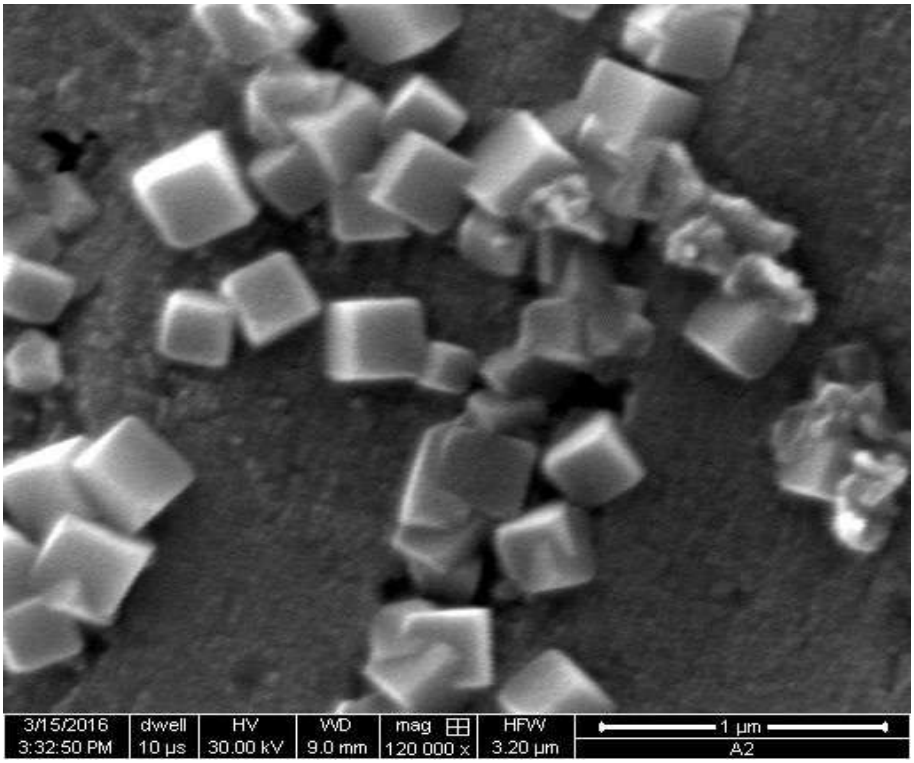

Figure 5.5d High resolution SEM image GO/MgO

The EDX analysis of the GO and GO/MgO nanocomposite is shown on Figure 5.6a and 5.6b. The image showed the distinct peak of C, O for GO and peaks of C, O, and Mg for the GO/MgO nanocomposite which revealed that the prepared GO and GO/MgO are highly purified. Furthermore, the EDX analysis of the GO/MgO after the lead adsorption was also performed which is given in Figure 5.6c. In this spectrum, the additional peak corresponding to the lead was also present along with peaks of C, O, and Mg which confirm the adsorption of lead on the GO/MgO surface. In order to study the distribution of different elements in the nanocomposite, the elemental mapping studies were also carried out. Figure 5.7a-c displayed the result of the analysis which suggested that the C, O, and Mg elements are uniformly distributed in the whole nanocomposite material which further supported the homogenous distribution of MgO nanoparticles on the GO surface.

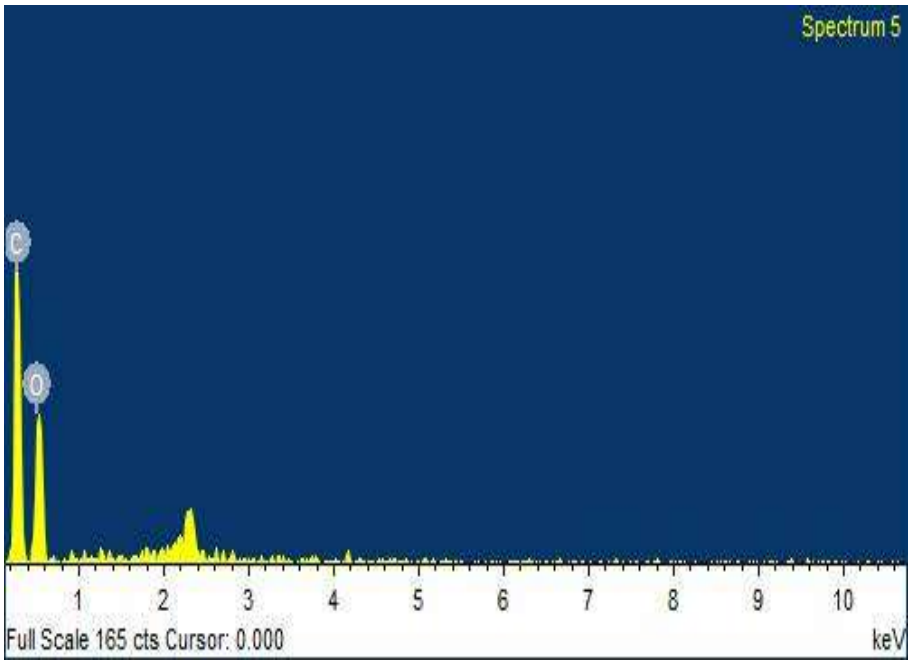

Figure 5.6a EDX spectrum GO

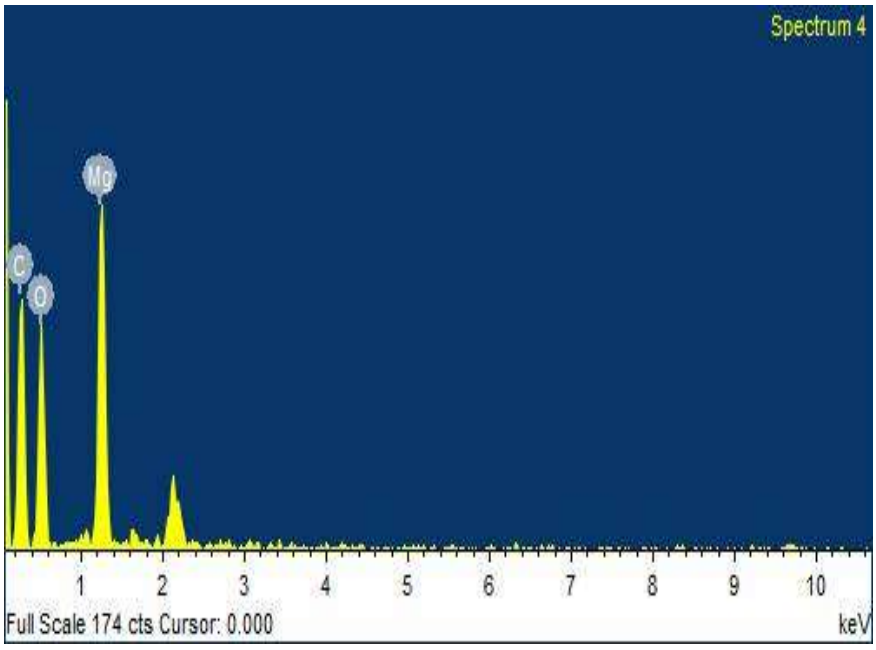

Figure 5.6b EDX spectrum GO/MgO

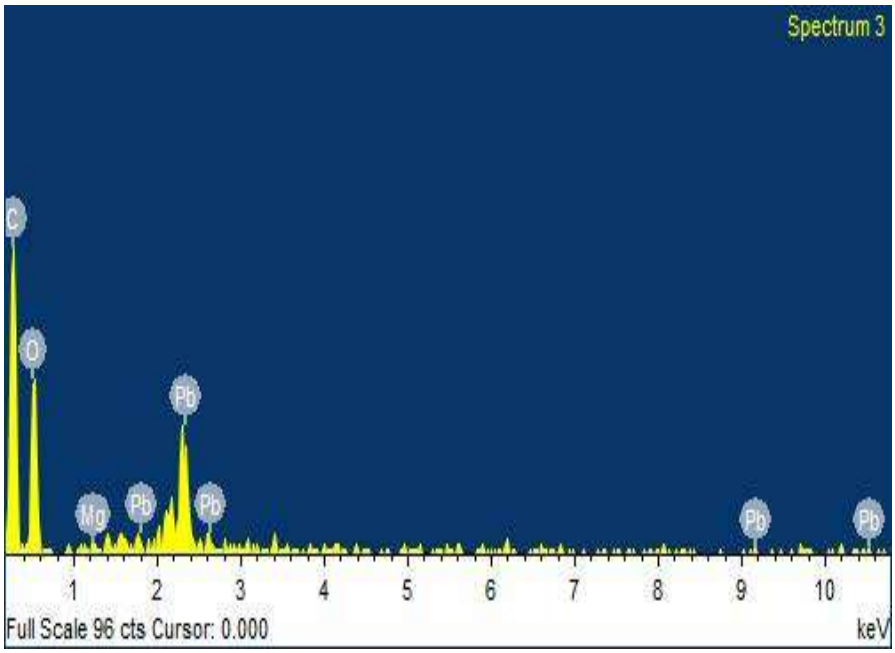

Figure 5.6c EDX spectrum GO/MgO after lead adsorption

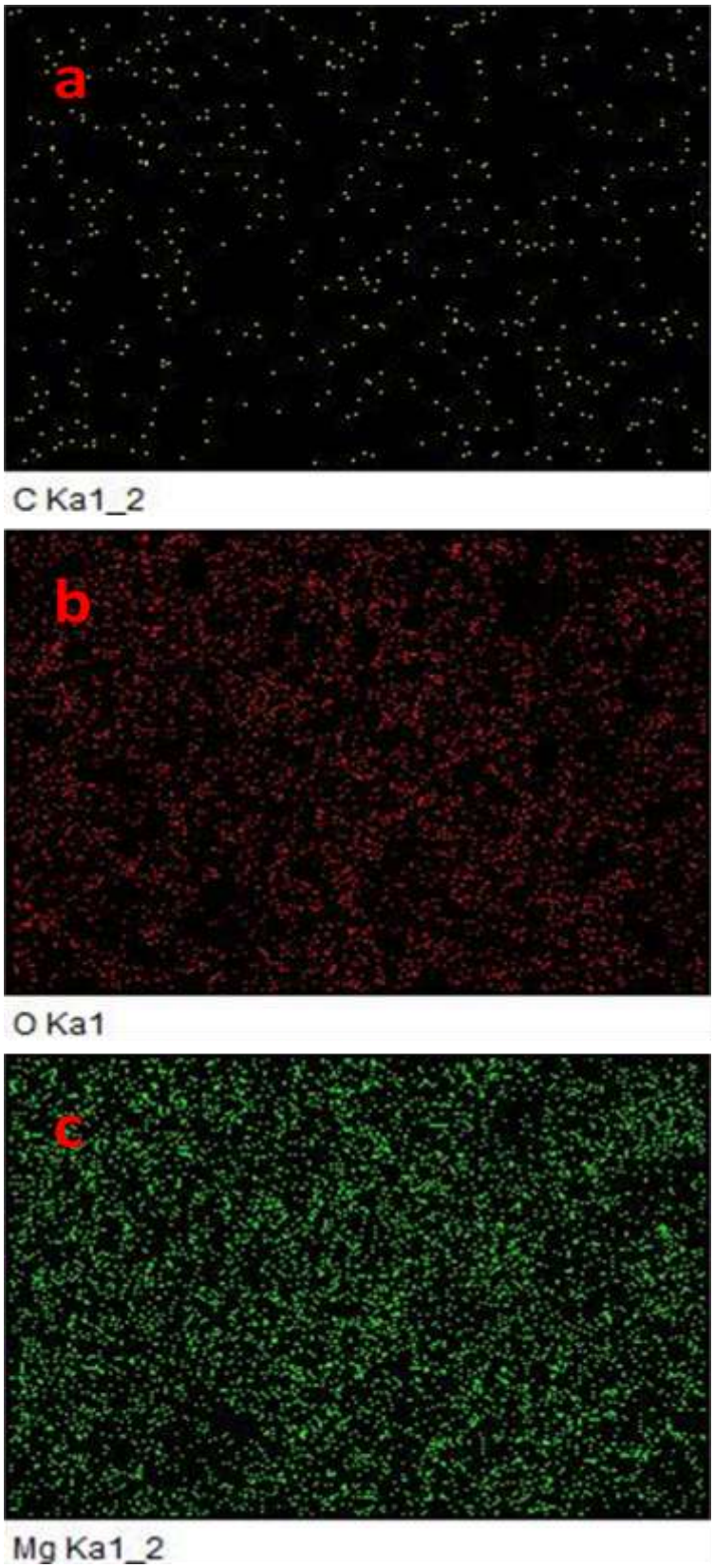

Figure 5.7 a-c Elemental Mapping analysis of GO/MgO

5.3.5 Raman Analysis

The results of Raman analysis of GO and GO/MgO is shown in Figure 5.8**.** Raman spectra of GO and GO/MgO nanocomposite were acquired from Renishaw in Via Raman spectrometer. The raman spectra of graphitic material reported to show the distinct band at 1351 cm^{-1} and 1582 cm^{-1} assigned to D and G band respectively [Sun *et al*. (2008), Ferrari (2007)]. In the raman spectrum of GO the D and G band located at 1343 cm^{-1} and 1587 cm^{-1} for the optical E2g in-plane vibration at the Brillouin zone center respectively [Pimenta *et al.* (2007), Zhu *et al.* (2010). Hence; the D band is used to measure the degree of defects in the carbon material. The D band shifted from 1343 cm^{-1} to 1356 cm^{1}, and the ratio of I_D/I_G increased from 0.93 to 1.007 due to the interaction of Mg^{2+} with the functional groups of GO.

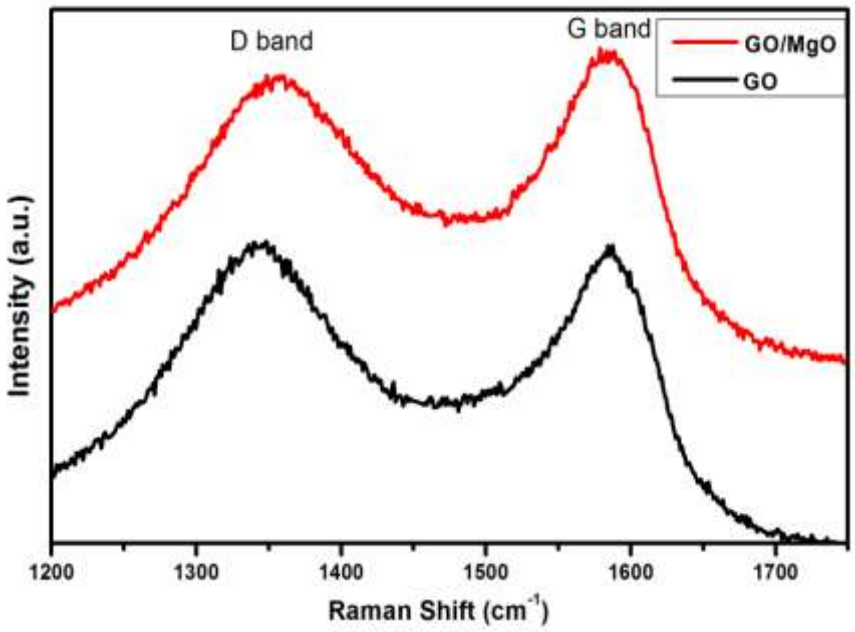

Figure 5.8 Raman spectra of GO and GO/MgO

5.3.6 Surface area measurement

Figure 5.9 represent the nitrogen adsorption-desorption isotherms curve for GO and GO/MgO. The curve showed the characteristic type IV nitrogen adsorption isotherm and displayed the H3 type hysteresis loop in the relative pressure [P/P_0] range of 0.3 to 0.97. The above results signify the mesoporous structure of the prepared GO/MgO nanocomposite [Luo *et al*. (2016)]. Further, the BET surface area of the GO and GO/MgO nanocomposite were observed to be 468 m^2/g, and 623 m^2/g respectively which is in the range (50−1300 m^2/g) of the surface area reported in the literature [Madadrang *et al.* (2012), Chandra *et al*. (2010), Park *et al.* (2011)]. The increase in surface area from GO to GO/MgO predicted that the nanocomposite formation would be beneficial for the lead adsorption due to enhanced surface area and more adsorption sites for the lead.

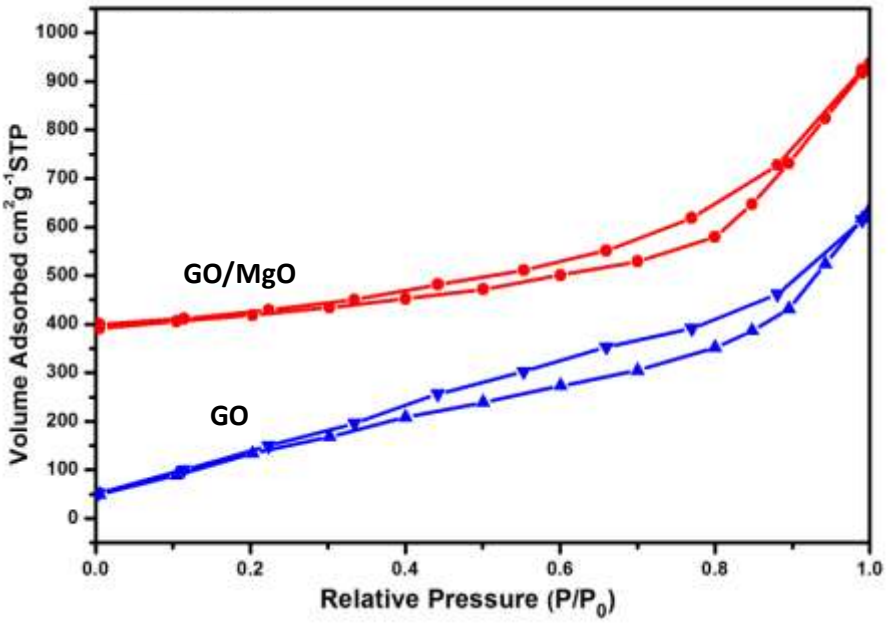

Figure. 5.9 BET curve of GO and GO/MgO

5.3.7 Determination of pHzpc

The zero point charge pH of the GO/MgO nanocomposite was determined by solid addition method which is given in chapter 2 in detail. The pHzpc was found to be at pH 6.0 at which adsorbent surface acquires the neutral charge. The typical curve of pH_i versus pH_f is shown in Figure 5.10

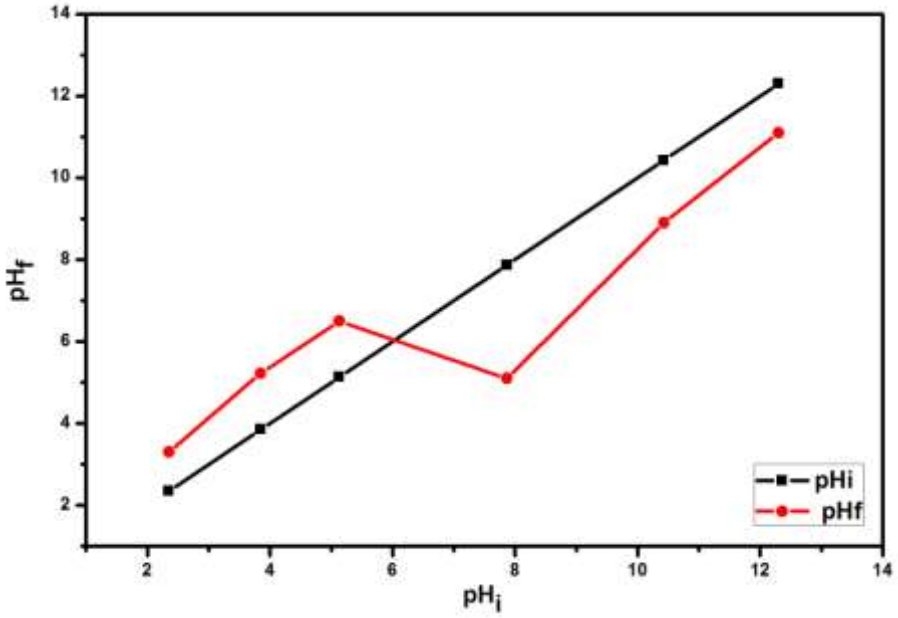

Figure 5.10 pHzpc curve of the GO/MgO

5.4 BATCH ADSORPTION RESULTS

5.4.1 Effect of pH and mechanism of lead adsorption

The pH plays a crucial role in the adsorption process as it affects the charges and states of the both the pollutant species as well as adsorbent species. Thus, in order to investigate the effect of pH on the lead adsorption, batch experiments were conducted at different pH varied from 2-10 whereas, all other parameters are kept

constant. Figure 5.11 showed that the uptake capacity was found to be increased with increase in pH values up to pH 7, and after that, it falls in further enhancement of the pH. This trend suggested that the uptake capacity of the GO/MgO is significantly affected by the pH change. The dependence of the adsorption capacity on pH of the system can be explained on the basis of aqueous chemistry.

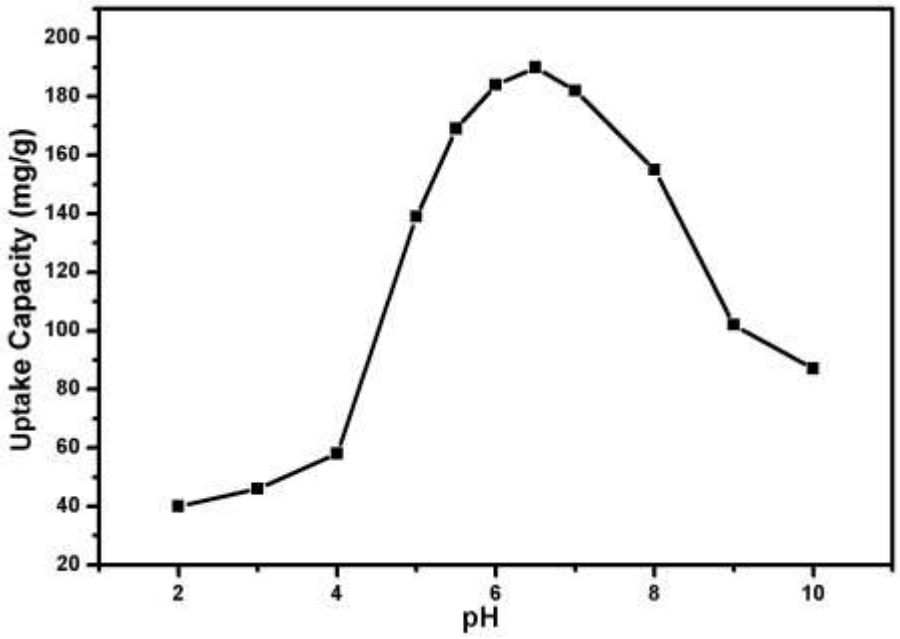

Figure 5.11 Effect of pH on the uptake capacity

During the adsorption process, the Pb^{2+} get exchanged with Mg^{2+} as well as H^{+}. Pb(II) exist in different ionic forms at different pH values such that Pb^{2+}, $Pb(OH)^{+}$, $Pb(OH)_2^{0}$, and $Pb(OH)_3^{-}$. In the higher pH range lead exist as a negatively charged species i.e. $Pb(OH)_3^{-}$. Therefore, it gets repelled by the negatively charged surface of the adsorbent which result in reduced uptake capacity at higher pH range [Zhao *et al.* (2011), Sheng *et al.* (2009)]. It is also important to mention here that in very low pH

the adsorbent gets protonated and become positively charged thus electrostatically repel the positive lead species Pb^{2+}. Hence; uptake capacity become lower at low pH. The range of pH from 4 to 7 is suitable for lead adsorption because in this pH range as the effect of protonation weakened and at the pH 6.5 adsorbent showed maximum adsorption capacity.

5.4.1.1 Mechanism of the lead adsorption

The prepared nanoadsobent (GO/MgO) contain two constituent, and both are actively participating in the adsorption process. Hence; adsorption mechanism of the lead removal involved two type of adsorption mechanism: (a) ion-exchange reaction between −COOH or −OH groups of GO with Pb(II) [Madadrang *et al*. (2012)] and (b)ion exchange reaction between Pb(II) and Mg(II) [Cao *et al*. (2012a)].

(a) Reaction of Pb(II) with −COOH and −OH groups of GO

It is well documented in the literature that various types of carbon based adsorbent have been used as an adsorbent for the abatement of heavy metal. Theses carbon adsorbents show superior adsorption capacity due to the presence of oxygen functional groups [Cao *et al.* (2012b)]. The oxygen functional groups make the adsorbent hydrophilic as well as also act as binding sites for the heavy metal ions [Madadrang *et al.* (2012)]. These functional groups certainly share their electron pairs in order to bind with Pb(II) to form complexes or may give up one proton during the ion exchange process [Chen *et al.* (2012)]. Figure 5.12 represent the schematic representation of the lead (Pb^{2+}) interaction with the GO. The above discussion can be illustrated in the form of following chemical equations [Chen *et al.* (2012)]:

$$GO - COOH + Pb^{2+} \rightarrow GO - COO^{-} - Pb^{2+} + 2H^{+} \quad (5.1)$$

$$(GO - COOH)_2 + Pb^{2+} \rightarrow (GO - COO^{-})_2 - Pb^{2+} + 2H^{+} \quad (5.2)$$

$$GO - OH + Pb^{2+} \rightarrow GO - O - Pb^{2+} + 2H^{+} \quad (5.3)$$

$$(GO - OH)_2 + Pb^{2+} \rightarrow (GO - O^{-})_2 - Pb^{2+} + 2H^{+} \quad (5.4)$$

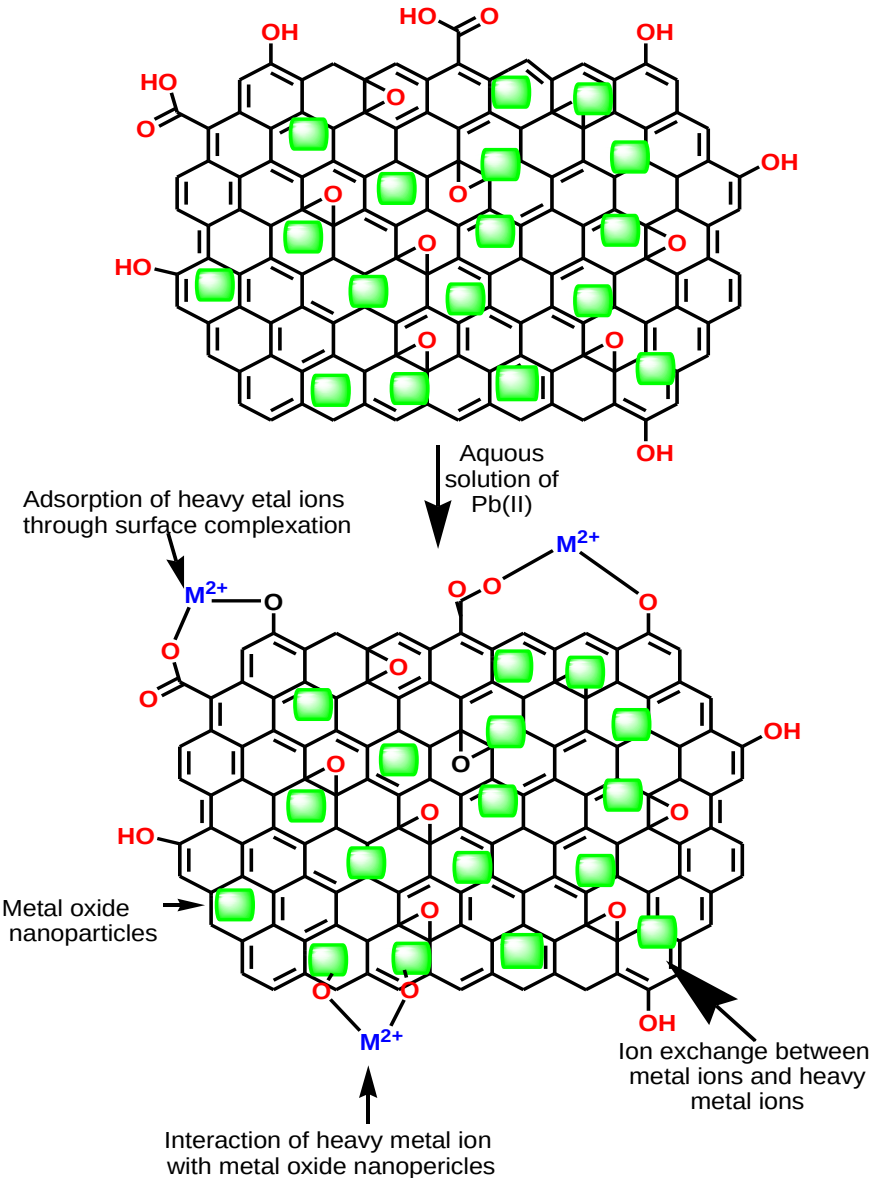

Figure 5.12 Schematic diagram representing the interaction of GO with lead

(b) Reaction of Pb(II) with MgO

In general, the adsorption mechanism of heavy metal involved the electrostatic interaction or ion exchange process. The literature supports the participation of hydroxyl group in the adsorption of anionic pollutant [(Upadhyay *et al.* (2014)] while this does not work well for the cationic pollutants. It was found that the concentration of Mg(II) increased in the solution after the adsorption Pb(II). The amount of Mg(II) increased with increase in uptake capacity. This result indicated that the Pb(II) exchanged with Mg(II) during the adsorption process. However, Mg(II) is the common metal cation which is present in the drinking water and its concentration in the treated water observed to be very low than the permissible limit (450 mg/L) set by WHO. During the adsorption process, Pb(II) exchange with the Mg(II) and resulted in the formation of PbO [Cao *et al.* (2012a)] this process can be illustrated by the solid-liquid interfacial reaction of Pb(II) with MgO.

$$MgO + Pb^{2+} = PbO + Mg^{2+} \quad (5.5)$$

The exchange of Pb(II) with Mg(II) was also supported by the XRD analysis of GO/MgO after lead adsorption (Figure 5.13). The XRD pattern shows the diffraction peaks corresponding to the PbO as well as MgO which were well matched with the JCPDS file no. 89-1589 and 89-7746 respectively. This study clearly demonstrated that the MgO partially reacted with the Pb(II) and the Pb(II) exchanged with Mg(II). Moreover, this exchange process was also proved by the core level XPS spectrum of Pb(II) (Figure 5.14) in which the characteristic peaks corresponding to the $4f_{7/2}$ and Pb $4f_{5/2}$ of PbO is present at 138.7 and 143.8 eV [Leelavathi *et al*. (2013)].

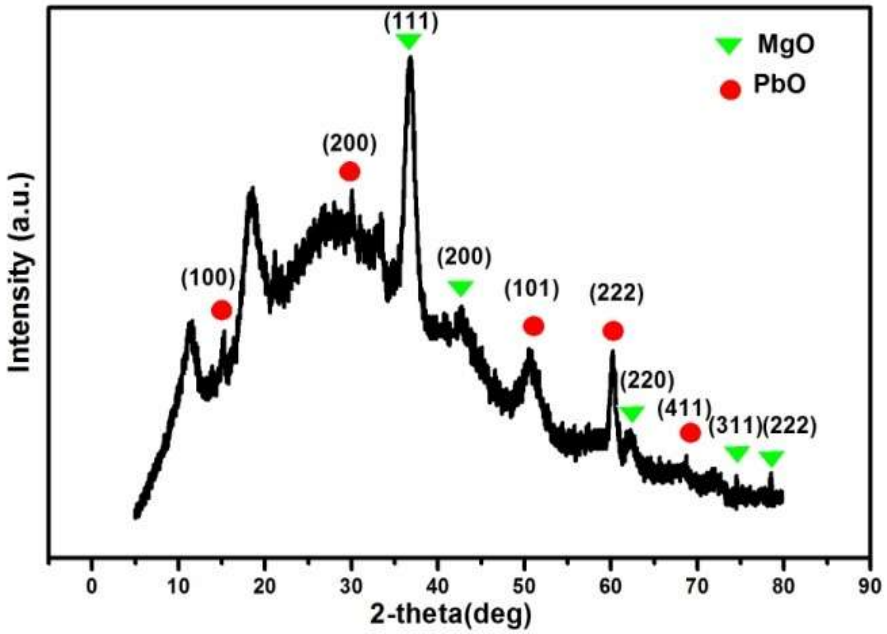

Figure 5.13 XRD pattern of GO/MgO after lead adsorption

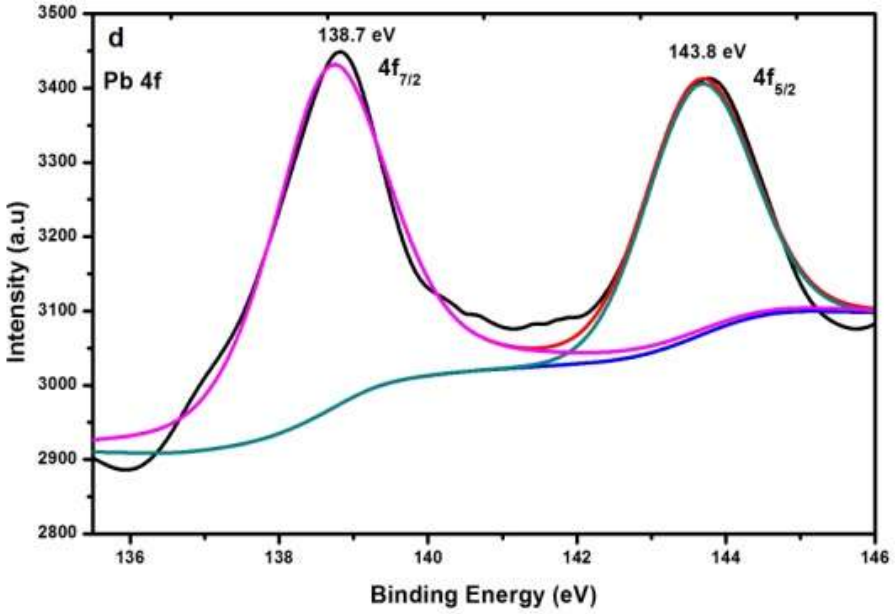

Figure 5.14 Core level XPS spectrum of Pb4f

5.4.2 Effect of contact time and GO/MgO dose on the uptake capacity

The effect of contact time and GO/MgO dose on the adsorption capacity was investigated at the lead concentration of 80 mg/L, pH 6.5, and temperature 30°C. The experiments were carried out at three different GO/MgO doses viz. 0.3, 0.4, and 0.5 g/L and the contact time was altered from 5 to 50 min. The variation of uptake capacity with the time and doses is represented by Figure 5.15. The results shows that initially, the adsorption occurred rapidly due to presence of abundant adsorption sites and high concentration of the lead. After some time adsorbent become saturated with the metal ions, resulted in the decline of uptake capacity. The reason behind the reduction in adsorption performance involved the lowered concentration gradient of lead and decline in available binding sites on the adsorbent. Furthermore, it was also observed that the optimum time for the achievement of equilibrium is 30 min for all the studied doses of GO/MgO thus, the contact time found to be independent of the GO/MgO dose. It was also revealed that the uptake capacity was also affected by the adsorbent doses. With the increase in GO/MgO dose from 0.3 t0 0.4 g/L the uptake capacity was also increased and attain maxima at 0.4g/L dose of GO/MgO. However, it decreased on further increase in dose from 0.4 to 0.5 g/L GO/MgO and this trend can be explained by the statement that the uptake capacity (mg/g) depends upon the ratio of adsorbate to the active binding sites which decreases with increase in adsorbent dose. Therefore, the uptake capacity of the GO/MgO reduced at the high adsorbent dose because the metal ion was unable to cover all the adsorption sites per unit mass of the adsorbent [Singh *et al.* (2016)].

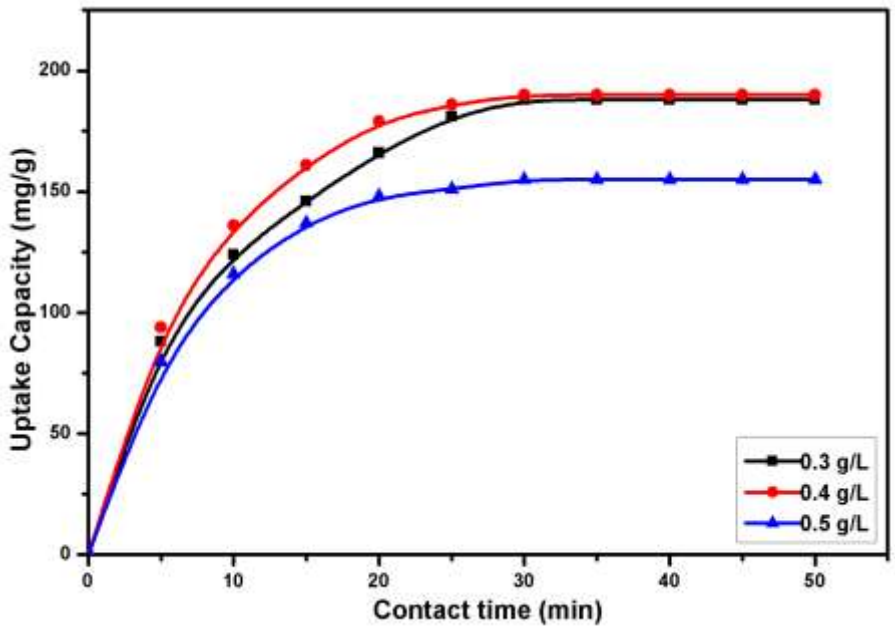

Figure 5.15 Effect of contact time and GO/MgO dose on uptake capacity

5.4.3 Effect of initial lead concentration and temperature on the adsorption

The effect of initial concentration of lead and temperature on the uptake capacity of the GO/MgO was investigated at different temperatures (20°C, 30°C, and 40°C). The experiments were carried out at constant pH (6.5) and GO/MgO dose (0.4 g/L) by varying the lead concentration from 20 to 160 mg/L. The results are presented in Figure 5.16 which suggested that uptake capacity was increased with the lead concentration up to the concentration of 80 mg/L. Further, no significant increase in uptake capacity was observed with increase in lead concentration. Therefore the 80 mg/L concentration of lead was sufficient to completely mask all the active adsorption binding sites of 0.4 g/L of the GO/MgO. The maximum adsorption capacity was found to be 190 mg/g at 30°C. The results revealed that the uptake capacity increased with the rise in temperature from 20°C to 30°C due to the formation of new binding sites. The new adsorption sites formed because of the breakage of some internal bond occurred at the high temperature [Singh *et al*. (2009)]. As the temperature increases beyond the

30°C, the adsorption capacity decreased because the randomness of ions enhanced in the solution which reduces the favorable effect of the temperature [Mohan *et al.* (2015)].

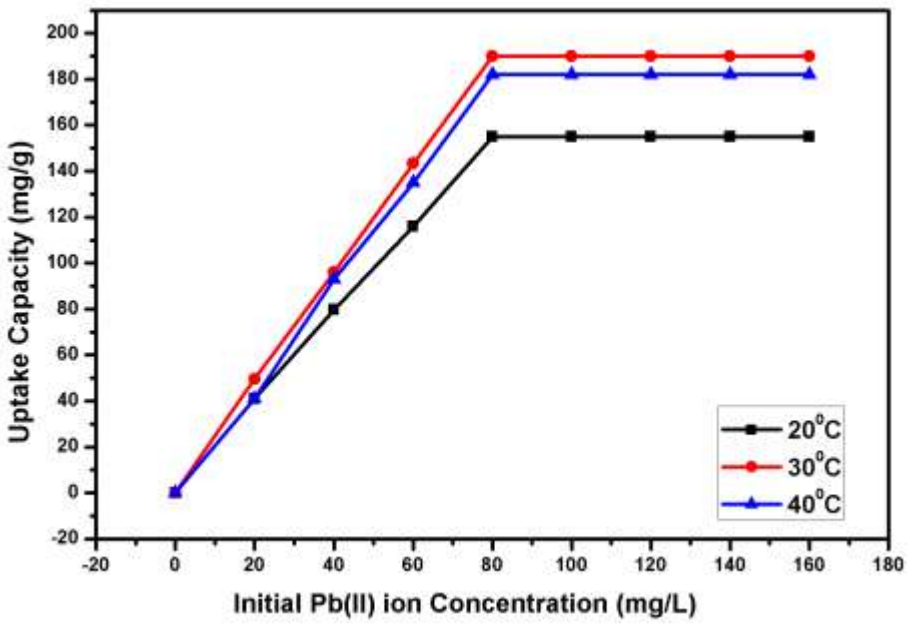

Figure 5.16 Effect of initial lead concentration and temperature on uptake capacity

5.5 Kinetic studies

The process of adsorption is strongly dependent on the time. Therefore, it is important to explore the kinetics of the adsorption system in order to design the treatment plant for lead removal. Thus, the information provided by the kinetic studies includes the rate of adsorption reactions and other important information which are necessary to design the efficient adsorption system. To explore the kinetics and adsorption mechanism of lead, different kinetics models were applied i.e. pseudo-first-

order, pseudo-second-order, mass transfer, Weber–Morris model, and Richenberg at three variable GO/MgO doses viz. 0.3, 0.4, 0.5 g/L. while pH and lead concentration kept constant at 6.5 and 80 mg/L respectively.

5.5.1 Pseudo-First-order kinetics and Pseudo-second-order kinetic

The plots of pseudo-first-order kinetics model at all the three doses are given in the Figure 5.17. All other parameter related with this model were determined form the slope and intercept of the graph of log (q_e-q_t) versus. t. It was observed that the plots of pseudo-first-order kinetics model at all the mentioned doses significantly deviate from the linearity which is also reflected by the low R^2 values (Table 5.1**)**. It was also found that the experimental and calculated values of q_e show contradiction which further suggested the non-applicability of the kinetic model for the adsorption of lead. Furthermore, in order to study the kinetics of adsorption, the experimental data were also subjected to the pseudo-second-order kinetics. The kinetic parameters were evaluated from the plots of t/qt versus t (Figure 5.18) and are listed in Table 5.1**.** The plots maintained considerable linearity at all the doses. The validity of the model also showed by the good agreement between the experimental and theoretical values of q_e. Hence, the pseudo-second-order kinetic model can better explain the adsorption of lead on GO/MgO [Konicki *et al.* (2013)].

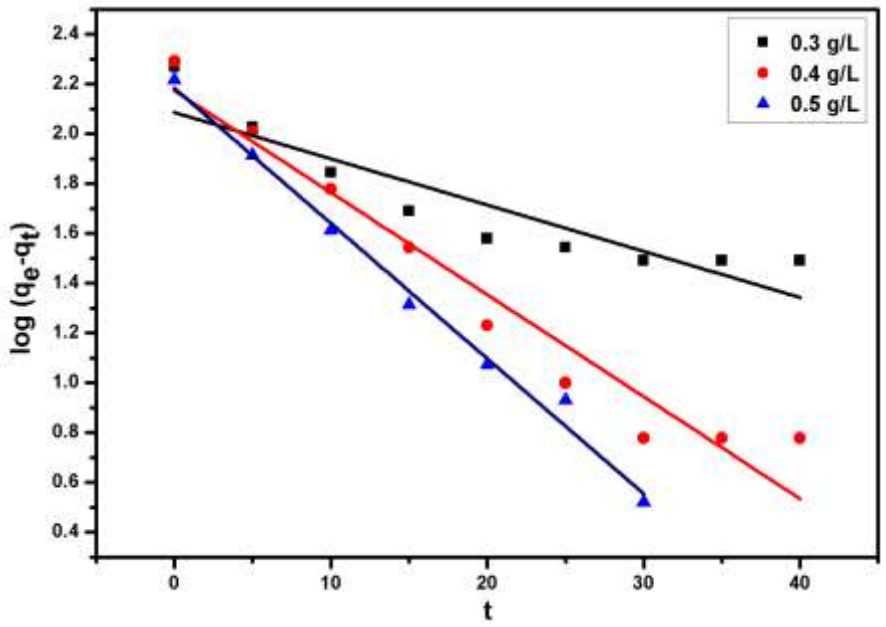

Figure 5.17 Pseudo-First-order kinetic plot

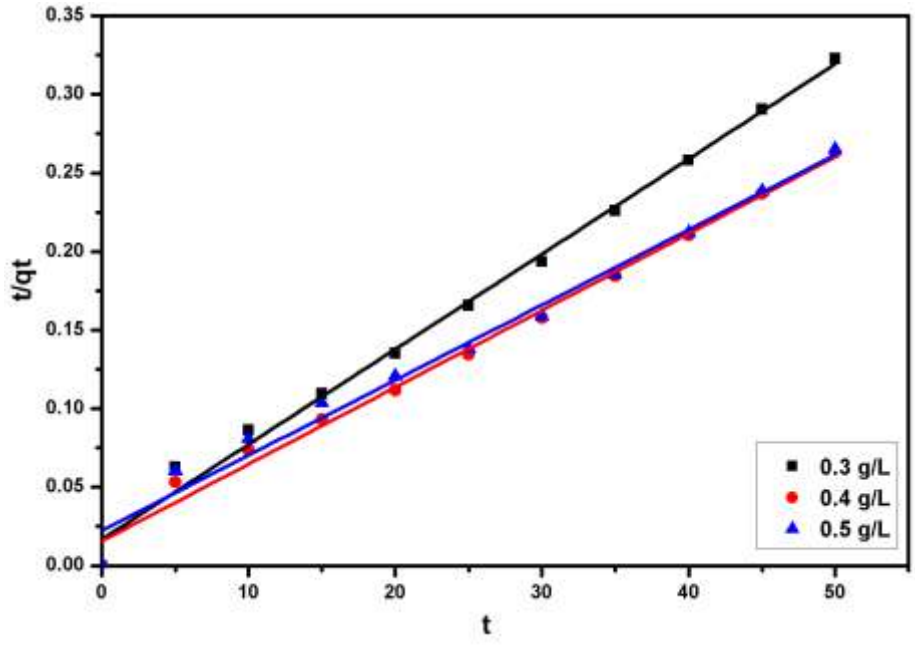

Figure 5.18 Pseudo-second-order kinetic plot

5.5.2 Mass transfer studies

The mass transfer plots of Mckay model at different doses for the lead adsorption by GO/MgO is represented as Figure 5.19. The experimental data fitted well with Mass transfer kinetic model which is supported by the high value of R^2 and significant linear plots at all the given doses. Thus, it indicated the existence of mass transfer process in this adsorption system. The mass transfer coefficient β_t (2.3×10^{-3}, 4.5×10^{-3}, 2.1×10^{-3}) of Mckay et al. model was calculated from the slopes of the plots of $\ln((Ct/Ci)-1/(1+mK))$ versus t (min) at different doses (0.4, 0.5, 0.6 g/L). The value of β_t observed to be very high which suggested the rapid mass transfer from boundary film to the adsorbent surface. Therefore, GO/MgO can be used for remediation of lead from water. Moreover, due to the high value of β_t, it was also concluded it cannot be considered as rate controlling step [Hasan *et al.* (2010)].

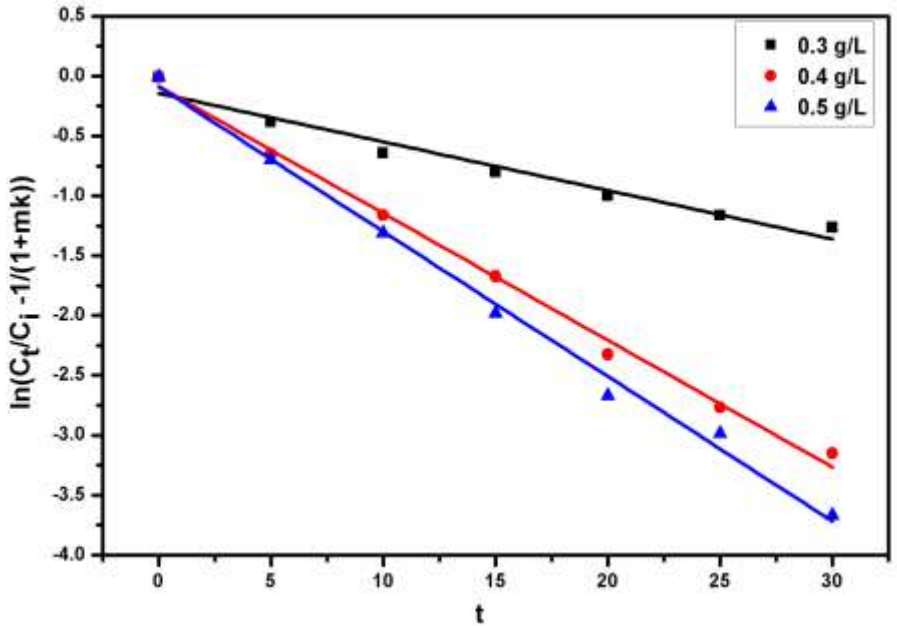

Figure 5.19 Maas transfer kinetic plot

5.5.3 Intra particles diffusion model

The plot of qt *vs.* $t^{0.5}$ (min) corresponding to the Weber-Morris model is shown in Figure 5.20 which is used to examine the probability of intraparticle diffusion in the adsorption process [Sharififard *et al*. (2016)]. For this adsorption system, the graph showed significant linearity at all the studied doses and other parameters of this model along with R^2 are listed in Table 5.1. The results showed that the values of R^2 are significantly high which recommended the validity of intraparticle diffusion of lead ions into the interstitial spaces and pores of the GO/MgO. The plots qt *vs.* $t^{0.5}$ found to be linear in a broad range of contact time but did not pass through the origin. It is well documented in the literature that when intraparticle diffusion solely acts as the rate controlling step, then the linear plot of qt versus $t^{0.5}$ must pass through the origin. Whereas, the deviation from the origin can be explained by the fact that there is two type of process which controls the rate of adsorption. Thus it can be concluded that initially, the boundary diffusion has taken part in the process of adsorption and later it was followed by the intraparticle diffusion process[Senthil Kumar *et al.* (2014)]. In addition, the intercept of the plot indicated the boundary layer diffusion effect, larger the value of the intercept, the larger is the contribution of the surface adsorption in the rate-limiting step. Overall this study confirms that the intraparticle diffusion was not solely determined rate of adsorption but it was one of them which also participate the rate determining step of this adsorption system. Therefore, the adsorption of lead on the GO/MgO nanocomposite involved more than one mechanistic pathways [Islam *et al.* (2010), Gupta & Bhattacharyya (2011)].

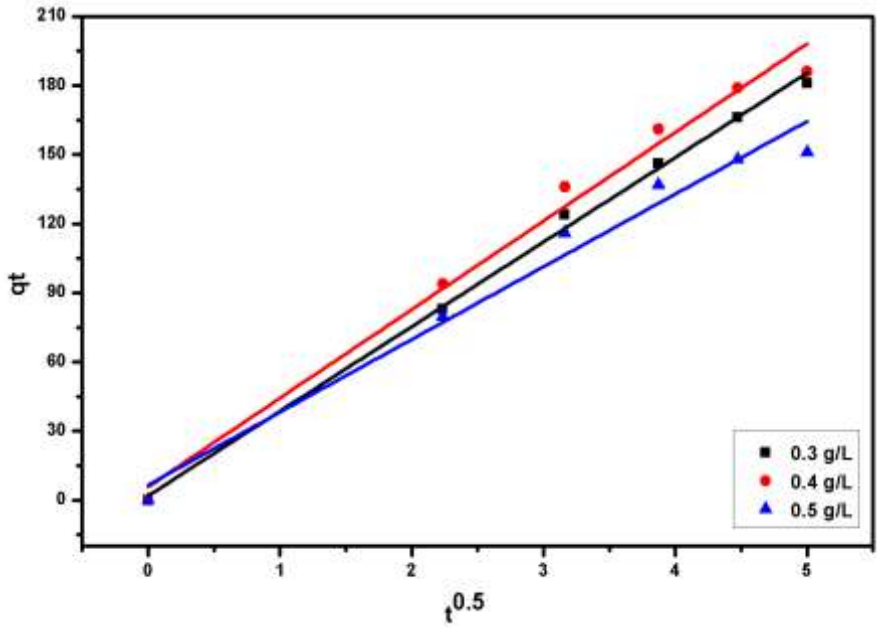

Figure 5.20 Intraparticle diffusion plot

5.5.4 Richenberg Model

Above discussion showed that the current adsorption process involves both mass transfer as well as intraparticle diffusion for the determination of the rate of reaction. Therefore, to explore the actual adsorption mechanism and for the identification of slowest step of the reaction, the experimental data was also applied to the Boyd kinetic model [Boyd and AW (1947)]. The Boyd kinetic model plots predict the important information about rate controlling step of the adsorption. It is a well-known fact that the intraparticle diffusion would be considered to be a rate limiting step if the plot observed to be linear and must be passed through the origin [Ranjan *et al.* (2009)]. However, for this adsorption system graph showed considerable linearity but did not pass through the origin which revealed that the only intraparticle diffusion was not involved in the rate determining step. This finding was well matched with the results of Weber-Morris model. The correlation coefficient (R^2) for linear plots of (B_t)

versus t (Figure 5.21) values at different GO/MgO doses are observed to be 0.9781, 0.9842 and 0.9905 at corresponding doses of 0.3, 0.4 and 0.5 g/L respectively. Hence; it is concluded that external mass transfer along with intraparticle diffusion played an important role in the determination of the rate of the reaction.

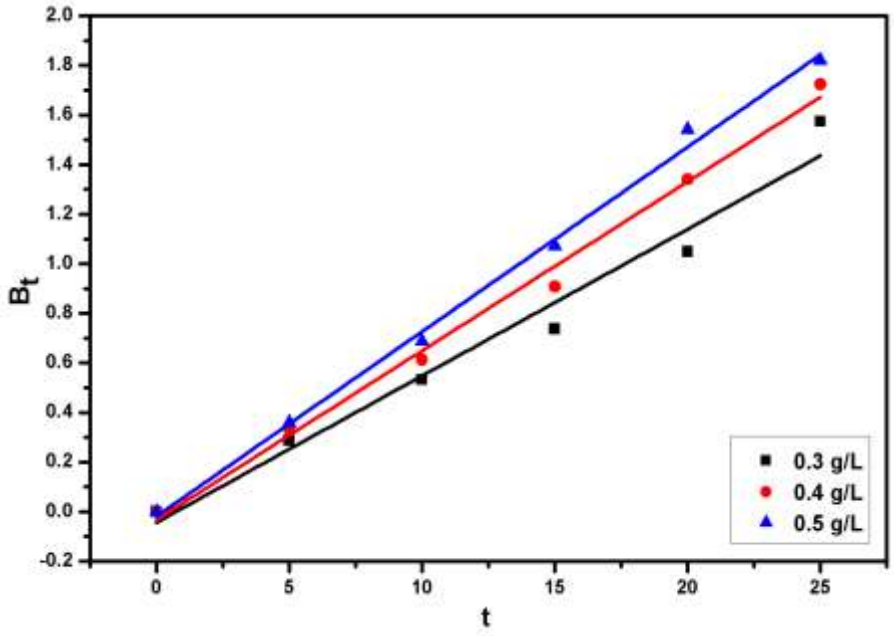

Figure 5.21 Richenberg Model plot

Table 5.1 Kinetic parameters for the adsorption of lead at different GO/MgO doses

Model Parameters	**lead concentration**		
	0.3g/L	**0.4g/L**	**0.5g/L**
Pseudo-first-order			
K_1 (min^{-1})	0.146	0.094	0.04
qe (exp.)(mg/g)	114.4	148	120.2
qe (cal.) (mg/g)	188.8	190	155
R^2	0.82	0.94	0.83
Pseudo-second-order			
K_2'	0.00012	0.00024	0.0034
qe (mg/g)	208.3	204	163
R^2	0.990	0.992	0.997
Mass Transfer			
$\beta_t \times 10^{-3}$ (cm^2/sec)	2.3	4.5	4.1
R^2	0.962	0.994	0.990
Intraparticles Diffusion			
K_{id}(mg/g.$min.^{0.5}$)	36.44	38.46	31.57
C	3.65	5.8	6.6
R^2	0.99	0.99	0.98

5.6 ISOTHERM STUDY

Adsorption isotherm study is a very important factor to understand the interactions between adsorbate ion and adsorbent. Thus, It is essential to establish an appropriate correlation of adsorption equilibria to optimize the adsorption system for effective adsorption of pollutant ions. For the present adsorption system, three isotherm models viz. Langmuir, Freundlich, and Dubinin–Radushkevich (D–R) were used to elucidate the adsorption equilibrium. The Langmuir and D–R isotherm proposed the monolayered adsorption, while the Freundlich assumes the multilayer adsorption. The isotherm studies were performed at different temperatures i.e. 20, 30, and 40°C by altering lead concentration from 20 to 160 mg/L.

5.6.1 Freundlich Isotherm

The plots of Freundlich isotherm (log q_e versus log C_e) at different temperatures is presented in the Figure 5.22. Table 5.2 summarized the values of Freundlich constants and R^2 values. The low R^2 value indicated that this isotherm model cannot effectively describe the current adsorption system. For this adsorption system, the values of n ranged in between 1 to 10 which suggested the beneficial adsorption of lead on the GO/MgO surface [Khan *et al.* (2015)]. Moreover, the k_f values also amplified with the rise in temperature which again indicated that adsorption system is endothermic in nature.

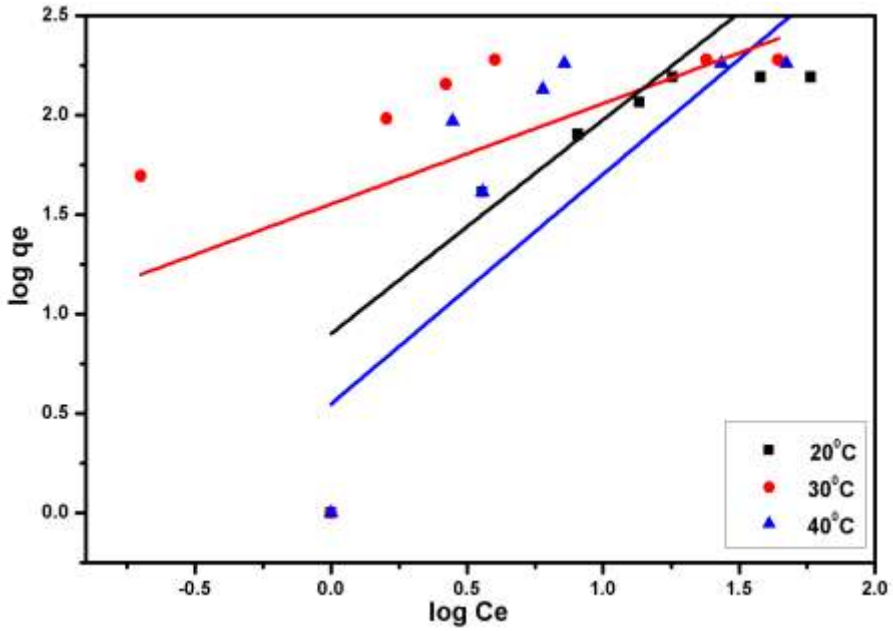

Figure 5.22 Freundlich Isotherm Plot

5.6.2 Langmuir Isotherm Model

The linear plots of Langmuir isotherm model at different temperature are shown in Figure 5.23 and the values of Langmuir constant along with R^2 are represented in Table 5.2. The values of b and Q° was calculated from intercepts and slopes respectively of the graph of C_e/q_e vs. C_e.. The experimental equilibrium data observed to be fit well with Langmuir isotherm model which is shown by the high value of correlation coefficients (R^2) (Table 5.2) which suggested its validity at all the studied temperature. The results recommended that the adsorption was monolayer and occurred on the homogenous active binding. The results also suggested that this adsorption process was endothermic in nature because Q° increased with the increase in temperature from 20°C to 30°C. The separation factor (R_L) was used to determine whether the adsorption was favorable or not. The R_L was calculated from the following equation:

$$R_L = \frac{1}{1+bC_0} \quad (5.6)$$

Where C_0 and b represent the initial concentration of Pb(II) and Langmuir constant respectively. The R_L value envisages the nature of adsorption i.e. favourable (0 < RL < 1) unfavourable (RL > 1), and irreversible (RL = 0) [Hasan *et al. (*2008)]. For the current adsorption system, the value of R_L was found to be 0.007 which indicated the favourability of this the adsorption system.

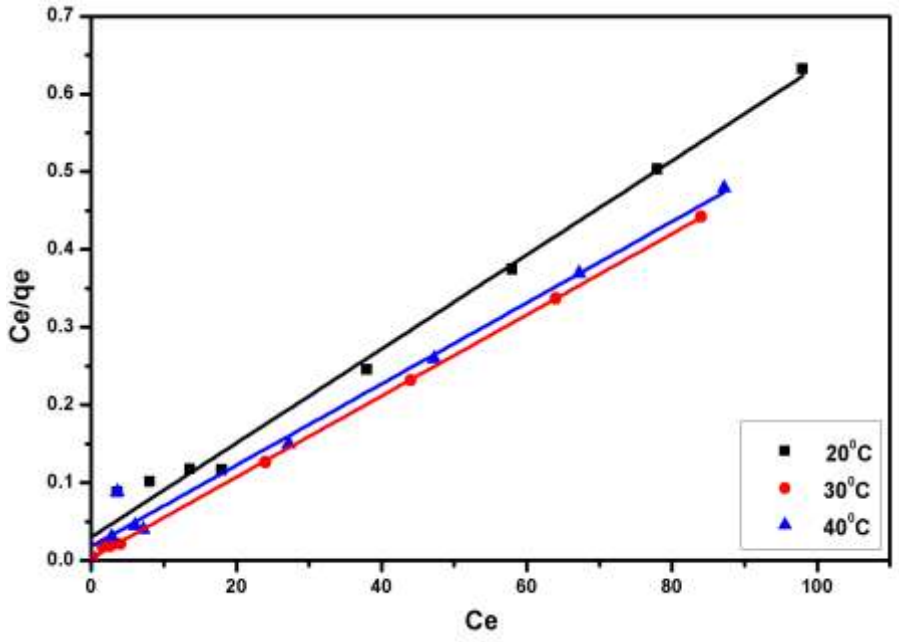

Figure 5.23 Langmuir Isotherm Plot

5.6.3 Dubinin–Radushkevich (D–R) adsorption isotherm

Dubinin–Radushkevich (D–R) adsorption isotherm plots (ln qe vs. F^2) is represented as Figure 5.24. For the present adsorption system, the D-R isotherm plots are linear at all studied temperatures, and the model fitted well to the equilibrium data. Table 5.2 listed all the important parameter of this isotherm and the high value of R^2 advocated for its applicability at all the temperatures. The value of E calculated and was

found to be in the range which is expected for chemical nature of adsorption. Therefore, it was concluded that the adsorption of lead on the surface of GO/MgO occurred via chemisorption process.

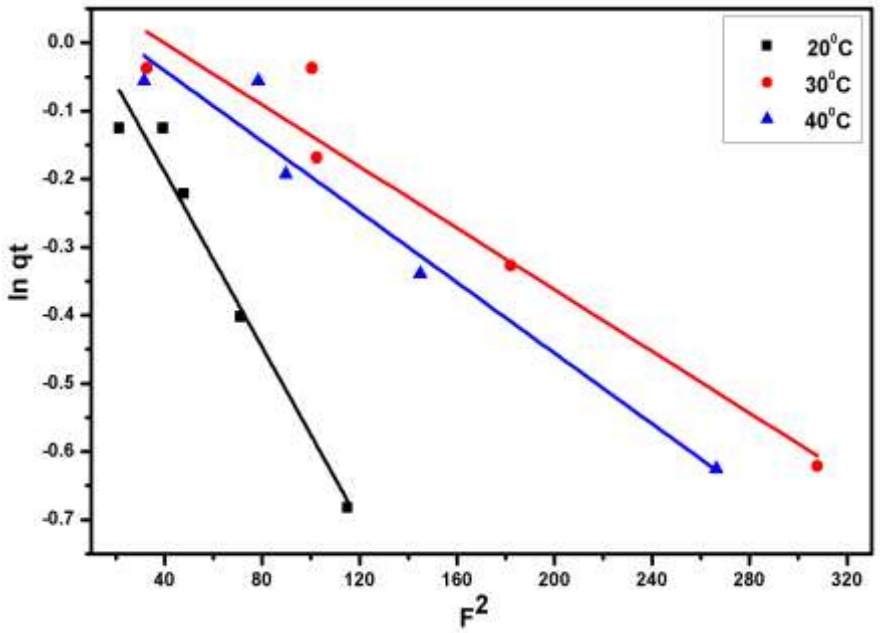

Figure 5.24 D-R Isotherm Plot

Table 5.2 Parameters of Langmuir, Freundlich and D-R isotherm for the adsorption of Lead at different temperature

Temperature	Freundlich Parameters			Langmuir Parameters			D-R Parameters		
	k_f (mg/g)	n	R^2	Q^0 (mg/g)	b (L/mg)	R^2	X_m (mmol/g)	E (KJ/mol)	R^2
20°C	5.1	1.1	0.72	163.93	0.204	0.99	1.03	9.13	0.97
30°C	36.3	2.3	0.74	196.07	1.75	0.99	1.055	15.43	0.95
40°C	11.48	1.3	0.56	192.30	0.305	0.98	1.049	14.14	0.95

5.7 Thermodynamic studies

The thermodynamic parameters (Gibbs free energy change(ΔG°), enthalpy change (ΔH°), and entropy change (ΔS°)) were calculated at 293, 298 and 303 K from the Van't Hoff plot (ln kc versuss 1/T) for the adsorption of lead on the GO/MgO which are summarized in Table 5.3 The value of R^2 is significantly high indicating that the plots are linear (Figure 5.25). The of ΔS° and ΔH° values were determined from the slope and intercept of the graph. The endothermic nature of this adsorption system was revealed by the positive value of ΔH° which was in good agreement with the findings of the isotherm study. The value of ΔG° was calculated to be negative which advocated the feasibility and thermodynamic spontaneity of the present adsorption system. It was also observed that the feasibility increased with the increase in temperature as can be seen by the more negative value of ΔG° at the higher temperature. The positive value of ΔS° indicated that the randomness is increased. Hefne et al. reported the same result and the reason behind the positive value of ΔS° which is due to the redistribution of energy between the adsorbate and the adsorbent [Hefne *et al.* (2008)]. The adsorbate was well-ordered in the vicinity of the adsorbent surface than in the consequent adsorbed state. As a result, with the increase in adsorption, the increase in the distribution of rotational and translational energy between some of the molecules occurred which cause to increase in randomness at the solid–liquid interface during the adsorption process [Kul and Koyuncu (2010).].

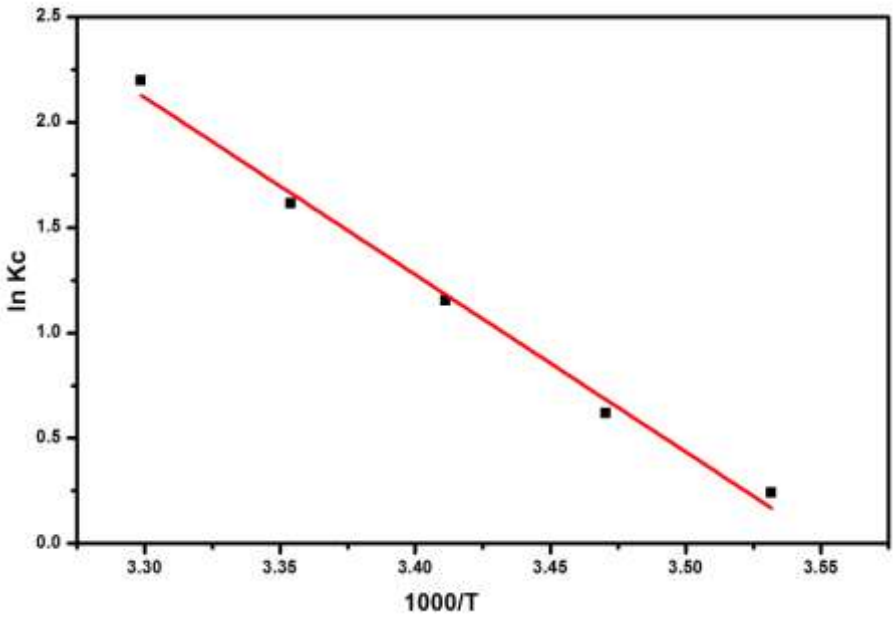

Figure 5.25 Van't Hoff plot

Table 5.3 Thermodynamic parameters for the adsorption of Lead on the GO/MgO

Temperature	ΔG(kJ/mol)	ΔH(kJ/mol)	ΔS(kJ/mol/ K)
20°C	-0.0056	0.1847	0.6334
25°C	-0.069		
30°C	-0.4699		

5.8 CONCLUSION

The novel nanocomposite GO/MgO was prepared by simple precipitation method which showed significant high adsorption capacity of 190 mg/g for lead from water at ambient temperature (30°C) and pH (6.5). This adsorbent has capacity for the removal of lead from the water without making much change in pH and temperature of the water. The adsorption equilibrium established in a very short period of time (30 min). The kinetic study of lead adsorption on the GO/MgO was also in support of the above fact because the experimental data fitted well with the pseudo-second-order kinetic model of adsorption. The external mass transfer and Weber-Morris kinetic models findings revealed that the intraparticle diffusion and external mass transfer both were actively participating in the rate determining step. The Boyd kinetic model also suggested that the intraparticle diffusion process was also involved in the rate controlling step. The Langmuir isotherm model fitted well to the equilibrium experimental data which indicates the monolayered adsorption. The findings of D–R isotherm model recommended that this adsorption process involved chemisorption behavior. Further, the thermodynamic studies discover that the adsorption was spontaneous and endothermic in nature. The optimum temperature for the lead adsorption by GO/MgO was found to be 30°C. Thus the lead adsorption by GO/MgO was cost effective and energy saving. The different data obtained from kinetics, isotherms, and thermodynamics studies from the batch experiments will be useful for the setup of continuous column system for the field application to treat lead-polluted water.